ATMOSPHERIC SCIENCE

Soil drought can mitigate deadly heat stress thanks to a reduction of air humidity

Hendrik Wouters[1,2]*, Jessica Keune[1], Irina Y. Petrova[1], Chiel C. van Heerwaarden[3], Adriaan J. Teuling[4], Jeremy S. Pal[5,6], Jordi Vilà-Guerau de Arellano[3], Diego G. Miralles[1]

Global warming increases the number and severity of deadly heatwaves. Recent heatwaves often coincided with soil droughts that intensify air temperature but lower air humidity. Since lowering air humidity may reduce human heat stress, the net impact of soil desiccation on the morbidity and mortality of heatwaves remains unclear. Combining weather balloon and satellite observations, atmospheric modelling, and meta-analyses of heatwave mortality, we find that soil droughts—despite their warming effect—lead to a mild reduction in heatwave lethality. More specifically, morning dry soils attenuate afternoon heat stress anomaly by ~5%. This occurs because of reduced surface evaporation and increased entrainment of dry air aloft. The benefit appears more pronounced during specific events, such as the Chicago 1995 and Northern U.S. 2006 and 2012 heatwaves. Our findings suggest that irrigated agriculture may intensify lethal heat stress, and question recently proposed heatwave mitigation measures involving surface moistening to increase evaporative cooling.

INTRODUCTION

In recent decades, more intense and frequent heatwaves have raised death tolls (1). European heatwaves, including the 2003 Western European and 2010 Russian events, accounted for 85% of all deaths caused by climate disasters in Europe between 1970 and 2012, with a total of over 120,000 reported lives (2). Observations suggest that extreme hot temperatures have become increasingly synchronized with drought conditions worldwide, as drier soils during heatwaves imply that an increased fraction of solar radiation is used to warm the atmosphere even further (3–7). Moreover, heatwave temperatures may be amplified through pulses of heat advection from anomalously dry regions upwind, as demonstrated recently for the 2010 Russian event (8). This connection to soil desiccation is partly responsible for the increasing frequency, intensity, and duration of heatwaves under global warming (9–12). Hence, it is widely assumed that soil dryness amplifies the adverse impacts of heatwaves. The potential lethality of heatwaves, however, is dependent not only on temperature but also on humidity; both increasing temperatures and increasing humidity burden human comfort, psychomedical health, and labor productivity (10, 11). This occurs because of the reduced capacity of the human body to regulate its temperature via perspiration as air humidity increases (1, 10, 13, 14). A recent consolidation of global human impact data confirms that the lethal temperature threshold decreases with increasing humidity (1), which remains consistent with many heat stress assessments based on various metrics (15).

Soil desiccation contributes not only to the escalation of heatwave temperatures (4, 9, 16–18) but also to the reduction in near-surface air humidity (19). Hence, the extent to which morbidity and mortality rates during heatwaves relate to soil drought is not self-evident. The effects of soil drought on air temperature (T) and humidity (q) act to counteract each other; the increased temperature is detrimental to human well-being, yet the reduced humidity is beneficial, especially if the individuals are well hydrated and in ventilated conditions. The implications are contrary for plants: Dry conditions during heat episodes are known to impose an additional source of stress, leading to the failure of the plant hydraulic transport (5, 20). For human health, however, not only is the influence of soil drought during heatwaves more ambiguous but also understudied. Previous work (e.g., 4–7, 21, 22) has highlighted the relevance of soil desiccation for the heatwave atmospheric boundary layer (ABL)—the air layer that is directly influenced by the land surface—but the relevance of these feedbacks for heatwave deadliness is unknown. Nevertheless, mitigation measures to offset drought and extreme high temperatures through increased evaporation, such as irrigation (23, 24), forestation (25), or urban green and water infrastructure (26, 27), have already been proposed. Especially, expanding irrigation is thought to have mitigated summer temperatures and exposure to hot extremes for over a billion people in recent decades (23). Yet, the knowledge gap regarding the influence of these mitigation measures on actual heatwave lethality hampers their evaluation: The cooling caused by these mitigation measures is deemed to benefit society but may still amplify human heat stress through increased air humidity (28).

Here, we quantify the net diurnal impact of soil dryness on lethal heat stress during heatwaves worldwide. To do so, we use a novel atmospheric modeling framework and a mortality-based human heat stress metric. A vast number of heat stress metrics have been developed over the past 50 years covering a wide range of sectors, regions, levels of complexity, input parameters, and spatiotemporal scales [e.g., (10, 11, 15)]. Building upon the concept of wet-bulb temperature (T_w)—a well-established physical metric that sets a thermodynamic upper limit of heat transport from a wet body to its environment—we design a function that fits the data from a recent meta-analysis of heatwave mortality (1). The new empirical "lethal heat stress" metric, T_s (Fig. 1A; Materials and Methods), incorporates the relation between T and q and global heatwave mortality while still remaining comparable to the physically based T_w metric. T_s enables us to scrutinize the influence of soil desiccation on deadly

[1]Hydro-Climate Extremes Lab (H-CEL), Ghent University, Ghent, Belgium. [2]Environmental Modelling Unit, Flemish Institute for Technological Research, Mol, Belgium. [3]Meteorology and Air Quality Group, Wageningen University & Research, Wageningen, Netherlands. [4]Hydrology and Quantitative Water Management Group, Wageningen University & Research, Wageningen, Netherlands. [5]Department of Civil Engineering and Environmental Science, Loyola Marymount University, Los Angeles, CA, USA. [6]Euro-Mediterranean Center on Climate Change and Ca'Foscari University, via della Libertà, Marghera, 12-30175 Venice, Italy.
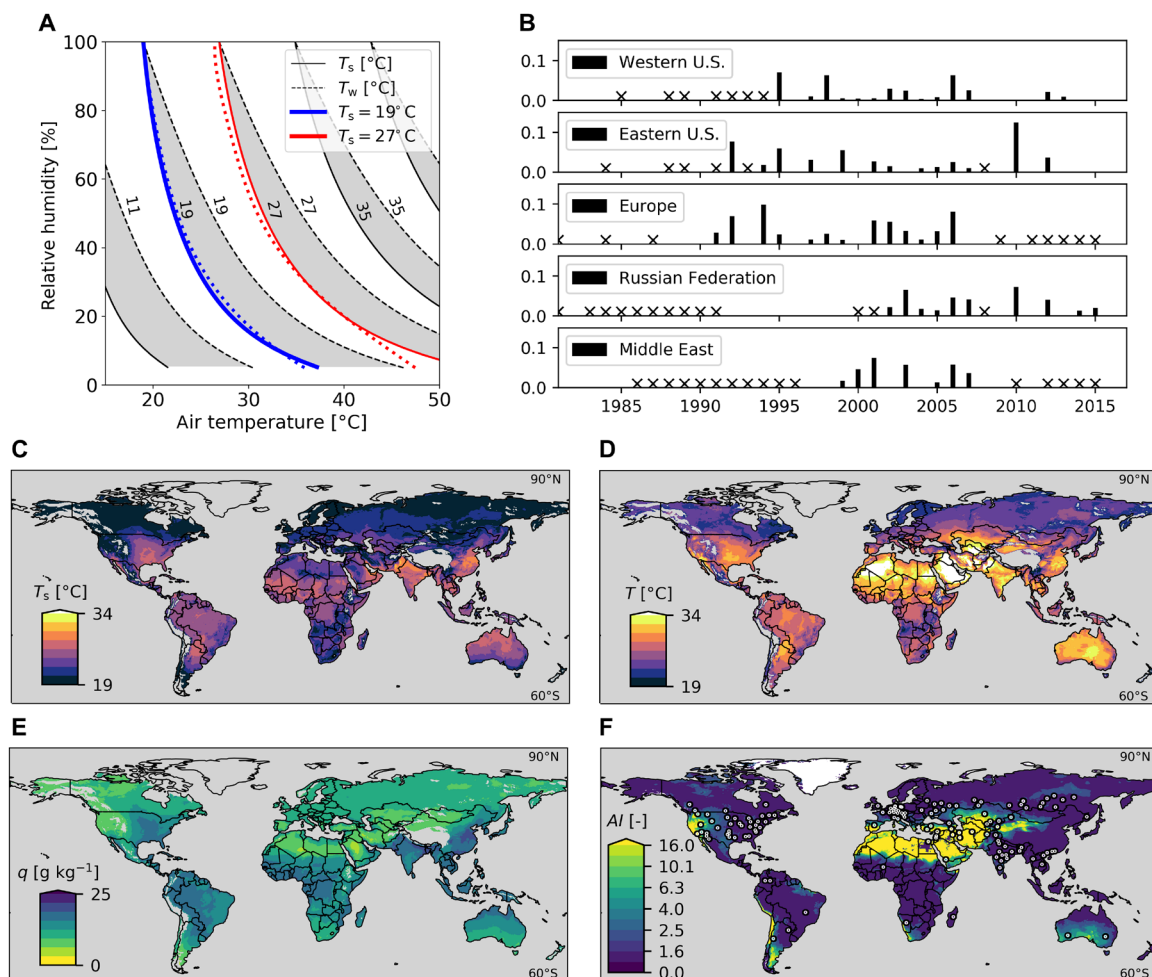*Corresponding author. Email: hendrik.wouters@ugent.be

Fig. 1. Human lethal heat stress as a function of temperature and humidity. (**A**) Comparison of daily human heat stress temperature (T_s; black full lines) to wet-bulb temperature (T_w; black dashed lines). The isopleths at $T_s = 19°C$ (blue continuous line) and $T_s = 27°C$ (red continuous line) closely correspond to lethal (blue dotted line) and deadly (red dotted line) thresholds, for which excess mortality is considered likely and certain, respectively. The gray shading highlights the difference between T_s and T_w for each plotted value. (**B**) Annual proportion of hot spell days to summer days with balloon soundings retained in the analysis. Hot spells are defined as days when daily mean T_s is equal to or higher than 19°C and the local 90th percentile value during summer (defined as the three consecutive months with the highest average T_s). Crosses indicate years with less than 25 days of summer soundings retained in the analysis (Materials and Methods). (**C**) Average daily T_s during hot spells, based on re-analysis data (47) from 1981 to 2015. (**D** and **E**) Corresponding average daily 2-m air temperature and specific humidity, respectively. (**F**) Climatological summer aridity index (ratio of average potential evaporation to precipitation) and global distribution of balloon soundings (dots) used in this study.

human heat stress across a range of climate conditions. Then, using a recently developed surface-atmospheric modeling framework, Chemistry Land-surface Atmosphere Soil Slab model for Global studies (CLASS4GL) (29), constrained by weather balloon observations (Materials and Methods), we quantify the net effect of soil moisture on T_s during hot spells worldwide. Model simulations are initialized in the morning, using data from summertime weather balloon soundings launched in different locations, and are then evaluated using the corresponding afternoon soundings. Subsequently, the effect of morning soil moisture levels on afternoon heat stress during hot spells is quantified. The simulated feedbacks include the effect of soil drought on heat stress via the interaction of the ABL with both land (evaporation and sensible heat fluxes) and free troposphere (entrainment of air from above the ABL). Given the increasing tendency of droughts and heatwaves to concur (3, 30) and jointly intensify each other (19, 31, 32), this understanding of the

contrasting effects of soil desiccation—not only through T but also through q—can be critical for predicting or mitigating future heat-wave lethality.

RESULTS

Global climate patterns during lethal hot spells

We first investigate the global distribution of T_s during hot spells. The World Meteorological Organization defines "hot spells" as episodes in which daily maximum (or minimum) T reaches its 90th percentile value (relative to all summer days) for three or more days in a row (33). Since our study focuses on days of heat stress for which excess mortality is likely, T_s, instead of T, is used to identify "lethal hot spells." To provide a sufficient sample size of weather balloon soundings meeting our quality criteria (see Materials and Methods), we also included single-day events. In addition to considering only days in

which T_s reaches the 90th percentile (relative to the three climatologically hottest consecutive summer months; see Materials and Methods), we only consider days in which T_s is greater than or equal to 19°C. The latter corresponds to the global "lethal" threshold in (1) from which excessive mortality is considered "likely" (see Fig. 1A). Last, daily mean values are used to define extremes instead of daily maxima (or minima), since the former has been shown to have a higher skill for identifying heatwave events with excess mortality (1). Applying these thresholds to balloon sounding data worldwide helps identify historical heatwaves such as those of 2010 in Russia and the Unites States, or of 1994, 2003, and 2006 in Western Europe (Fig. 1B). As expected, the global distribution of T_s reflects the magnitude of T (Fig. 1D) and q (Fig. 1E). Over extremely hot regions, such as the Sahel and the Arabian Peninsula, T_s is lower than T because of the offsetting impact of air dryness (Fig. 1, D to F). In countries such as India and China, T_s better reflects the distribution of q despite the comparatively low T (Fig. 1, D to F). High q areas in East and South Asia approach and exceed the threshold of $T_s = 27°C$, at which the risk of excess mortality is considered "certain" in (1).

Anomalies in T_s during lethal hot spells (Fig. 2A) coincide with anomalously high T (Fig. 2B) and q (Fig. 2C). In the case of mid and high latitudes (>45°N and >45°S), anomalies in T_s also concur with low soil moisture (Fig. 2D). The synchronization of high T_s and anomalously dry soils reflects the well-known effect of drought on escalating T (4, 16, 34). The correspondence between dry soils and high T holds across different levels of aridity (Fig. 1C); yet, it is predominant in part of the tropics (from 20°S to 10°N) and mid latitudes. Air humidity (q) appears less coupled to the land surface conditions than air temperature (T) since for most high latitudes (>60°N and > 60°S), the excess q during lethal hot spells (Fig. 2C) still appears in association with anomalously dry soils (Fig. 2D). We emphasize that the correspondence of anomalously high T_s (Fig. 2A) and dry soils (Fig. 2D) in mid- and high-latitude regions does not necessarily indicate a positive causal link between the dry soils and the peaks in T_s. Moreover, the relation between soil moisture and T_s anomalies is less pronounced, and even reversed, in arid regions where abnormally moist soils (and air) concur with anomalous lethal heat stress (compare Fig. 2D and Fig. 2A). This is the case for central Australia,

Arabian Peninsula, Sahel, or Namib Desert, suggesting an aggravating effect of soil wetness on human heat stress via increased evaporation (and thus air humidity) in these arid regions. Nonetheless, the patterns shown in Fig. 2 only reflect covariant anomalies in these variables and not actual causation.

Land-atmosphere drivers of lethal heat stress

To quantify causal relationships and decipher the complex role of soil desiccation on human heat stress via air temperature and humidity, we use a recently developed atmospheric modeling framework, CLASS4GL (29) (Materials and Methods). Using worldwide morning balloon soundings to initialize the model, the diurnal cycle of the ABL is simulated, constrained by satellite and reanalysis data describing atmosphere and land conditions, and especially soil moisture (29, 35). The framework allows us to infer the diurnal sensitivity of the ABL to the fluxes of heat and moisture from above (free troposphere) and below (land surface), as well as to horizontal advection of heat and moisture. Hence, the effect of soil desiccation on the T and q of the ABL during lethal hot spells can be inferred. To do so, we replace the soil moisture during hot spells with the median summer soil moisture and rerun the diurnal simulations. The analysis is based on 10,517 morning-afternoon pairs of weather balloon profiles at 60 stations distributed worldwide (see Fig. 1F for the location of the soundings).

The mean anomalies in afternoon T and q during hot spells are of +5.5°C and +2.1 g kg^{-1}, respectively (black bars, Fig. 3, B and C), yielding a mean anomaly in T_s of +3.7°C (black bars, Fig. 3A). In some cases, the T, q, and T_s anomalies are already evident in the morning and stem from the large-scale atmospheric flow patterns and land-atmospheric interactions from preceding days (4) (see dotted bars in Fig. 3). Although the framework only considers impacts over diurnal time scales, starting the day with the actual (low) soil moisture leads to an additional +0.55°C of afternoon warming (orange bar in Fig. 3B) or 10% of the T anomaly (compare orange bars with thick rectangles in Fig. 3B). Despite the anomalously wet air observed during lethal hot spells, the concurrence of dry soils causes atmospheric drying of 0.45 g kg^{-1} (orange bars in Fig. 3C) or an attenuation of q anomalies by −21% (compare orange bars with thick rectangles in
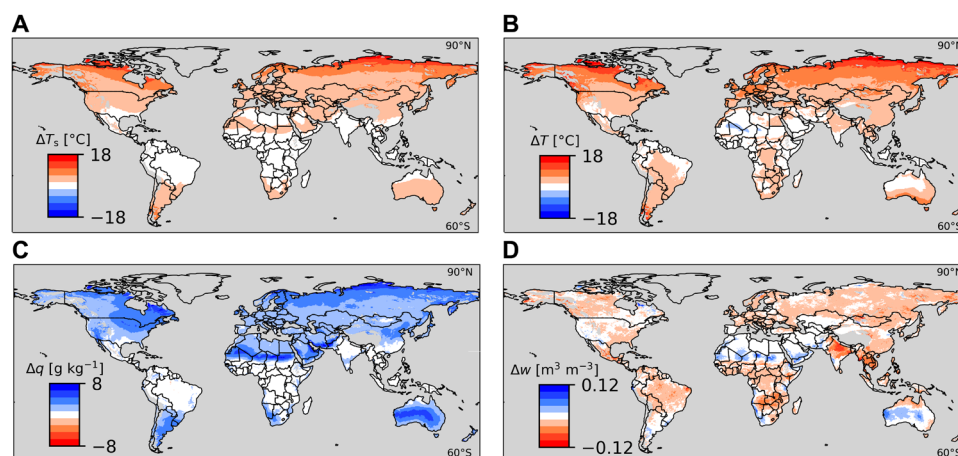

Fig. 2. Heat stress anomalies during lethal hot spells. Departures of hot spells compared with the summer climatology for (**A**) human heat stress temperature ΔT_s, (**B**) air temperature ΔT, (**C**) air humidity Δq, and (**D**) root-zone soil moisture Δw, according to reanalysis (47) (A to C) and satellite-based soil moisture (51, 52) (D) data (1981–2015).
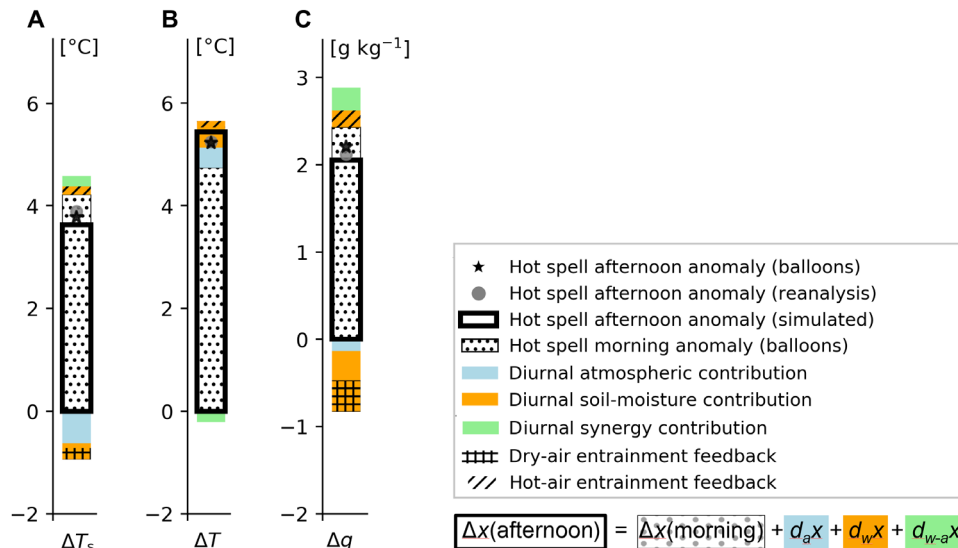
Fig. 3. Land-atmosphere drivers of human heat stress. Anomalies of (**A**) heat stress temperature ΔT_s, (**B**) air temperature ΔT, and (**C**) specific humidity Δq during hot spells relative to the average climatological summer. These are based on 10,517 morning-afternoon pairs of weather balloons over 60 stations (black stars), reanalysis data (gray dots), and observation-driven atmosphere modeling (black boxes). The observed anomalies in the afternoon (3:15 p.m. local time on average) are subdivided into the already present morning anomaly (4:40 a.m. local time on average; dotted bars), the diurnal atmospheric contribution ($d_a x$; blue bars), the diurnal soil moisture contribution ($d_w x$; orange bars), and the "synergy" contribution ($d_{w-a} x$; green bars; Materials and Methods). Hatched (crossed) boxes represent the influence of the entrainment of dry (hot) air from the free troposphere.

Fig. 3C). The atmospheric drying and heating by soil desiccation are more (less) pronounced in regions of lower (higher) aridity (fig. S7, B and C), likely due to the larger (smaller) soil moisture anomaly in those regions (see the Supplementary Text).

While the anomalies in T and q are both positive during human heat stress events (Figs. 2, B and C, and 3, B and C), the coinciding soil drought lowers q (orange bars in Fig. 3C), which counteracts the detrimental influence of soil drought on heat stress via T (orange bars in Fig. 3B). The elevated T and decreased q in response to soil desiccation are induced by an increase in surface-sensible heat and a decrease in evaporation (*4*, *19*). This direct surface influence (non-dashed orange bars in Fig. 3) also entails an upper-air feedback (see dashed orange bars in Fig. 3), which arises from the larger ABL growth due to the enhanced convective turbulence as the air is warmed from below. This extra ABL growth causes additional entrainment of warm and dry air from the free atmosphere (*4*, *36*) and exacerbates the overall heating and drying of the lower atmosphere by soil desiccation, which is a typical process during mega-heatwaves (*4*). The overall influence of soil dryness on hot spell lethality is explored in the following section.

Compensatory impacts of soil desiccation on human heat stress

The net impact of soil dryness on human heat stress during hot spells is analyzed by considering land-atmosphere feedbacks at every sounding location, using T_s as a diagnostic of human heat stress (Fig. 4). Soil dryness during hot spells shows a net beneficial influence globally. On the one hand, the afternoon T during lethal hot spells is +0.55° ± 0.60°C (average ± range encompassing minimum and maximum value across all aridity classes) higher because of the concurrent dry soils (Figs. 3B and 4A, and fig. S7A), which translates into a +0.12° ± 0.13°C increase in T_s (Fig. 4B). The changes in T cause

only a mild change in T_s since the latter depends also on q, and, in addition, higher T by itself implies a reduction RH, which partly attenuates the increase in T_s (fig. S5). On the other hand, q decreases by −0.45 ± 0.50 g kg^{-1} because of the concurrent dry soils (Fig. 4A), which translates into a −0.28° ± 0.29°C decrease in T_s (Fig. 4B). This reduction in human heat burden stems from the associated decline in relative humidity (fig. S5). As a result, the dry soils characteristic of lethal hot spells cause an overall reduction in T_s of −0.16° ± 0.18°C, which means −5 ± 5% of the T_s anomaly (Fig. 4B). Overall, the dry and hot air entrainment feedbacks in response to the extra ABL growth (see previous section) also compensate each other and slightly contribute to the overall reduction in T_s (Fig. 3A). These findings are consistent with the expected reduction of moist static energy—the sensible heat (or temperature multiplied by the specific heat c_p) of an air parcel after condensation of the water vapor content—in response to ABL growth (*11*, *37–39*).

During the events in which the risk of excess mortality is considered as certain by (*1*), associated with T_s > 27°C (see Fig. 1A), the benefit of having dry soils in the morning is generally amplified, leading to a reduction of −0.19° ± 0.12°C (median ± interquartile range over the extreme cases with anomalous dry soils) in afternoon T_s (see $d_w T_s$; Table 1). The beneficial effect varies largely from event to event, as revealed after investigating the most severe heatwaves: Chicago in 1995 (between −0.05° and −0.32°C), Northern U.S. heatwaves of 2006 and 2012 (between −0.14° and −0.36°C), Dallas 1997 (−0.17° and −0.21°C), India in 2002 (−1.71°C), and United States in 2010 and 2021 (−012° and +0.36°C). A minority of events, such as the Eastern U.S. 1999 and Asia 2007 hot spells, experienced wet instead of dry soil anomalies; in those cases, considering climatological soil moisture values leads to an increase in T_s (between +0.04° and +0.14°C, and +0.08 °C, respectively) (Table 1). It is important to note that due to limitations related to the timing of sounding measurements
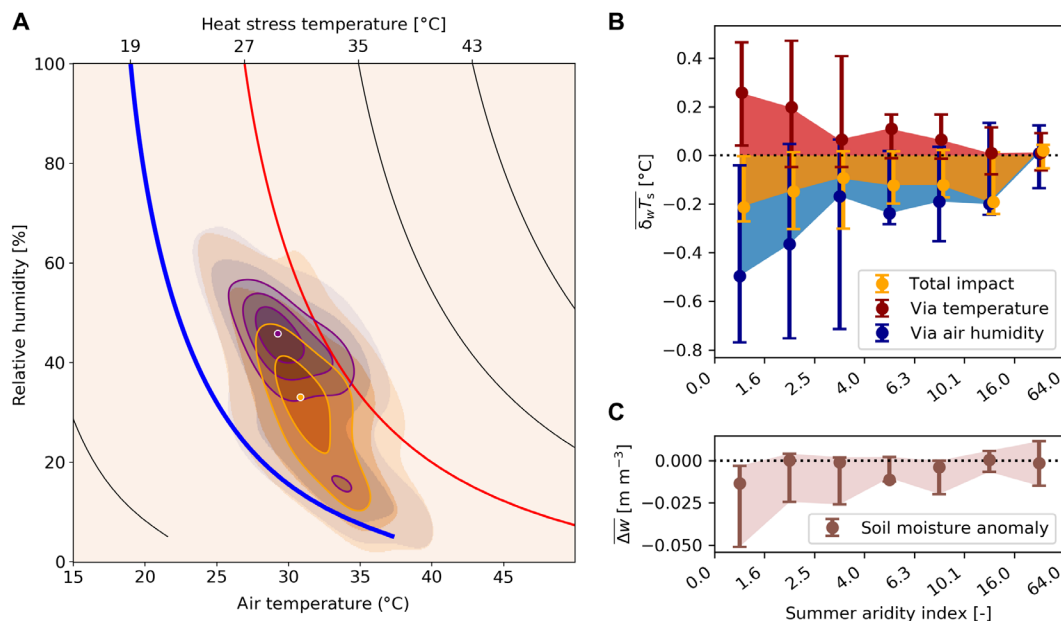
Fig. 4. Impact of soil drought on heat stress during lethal hot spells. (**A**) Density distribution of afternoon heat stress temperature T_s during hot spells considering the concomitant anomalous soil moisture levels (orange fill) and considering the soil moisture median of its summer climatology (purple). Contour lines highlight the highest densities, and the purple and orange dots indicate the maxima of the distributions. The isopleths at $T_s = 19°C$ (blue line) and $T_s = 27°C$ (red line) closely correspond to the lethal and deadly threshold from (1), respectively. (**B**) Variation of soil moisture impact on afternoon T_s as a function of aridity (summer average potential evaporation divided by precipitation), considering the total effect (orange), only the afternoon temperature change (red), and only afternoon air humidity change (blue). (**C**) Soil moisture anomaly during hot spells. The error bars in (B) and (C) indicate the interquartile ranges among the analyzed hot spell days.

during the day, some regions such as the Middle East and Europe have a lower representation in the analysis than other regions such as the United States (Fig. 1B). While the net beneficial influence of concurrent dry soils on heat stress can largely vary from event to event, as shown for the cases above, the overall benefit remains consistent when averaged over aridity clusters (Fig. 4B). The low variability across different aridity levels occurs even though soil dryness anomalies during lethal hot spells tend to be less pronounced in arid regions (Fig. 4C). Both the detrimental effect via T and the beneficial effect via q decrease with increasing aridity at the same rate (see also the Supplementary Text for more information).

DISCUSSION

Heatwaves and droughts are projected to occur more frequently in association, as compound events (31). Yet, an understanding of the impact of soil desiccation on human heat stress still needs to be developed. The outcomes of our study highlight that soil drought modestly reduces lethal heat stress at diurnal time scales. Hence, the reduced levels of air humidity associated with drought can play a beneficial role, which outweighs the detrimental role via increased air temperature. The reliability of this conclusion lies in the veracity of the proposed heat stress diagnostic (Fig. 1A). While the metric mimics the degree to which air humidity and temperature affect human health according to recent meta-analyses of mortality data during heatwaves (1), our results still depend on the resulting weighting between temperature and humidity in that metric. To test the robustness of the results, we repeat the analysis using the commonly used T_w and the simplified wet bulb globe temperature (sWBGT) (15). Both metrics ratify our findings, indicating an even less ambiguous benefit of soil

dryness against heat stress (compare figs. S9 and S10 with Fig. 4B). The lower weighting of RH introduced in T_s to better reflect the lethal aspect of heat stress as captured in (1) implies that our findings are conservative regarding the potential benefits of dry soils. In the case of extreme hot spells ($T_s > 27°C$), the findings are again clearer when T_w is used as diagnostic of heat stress (see Table 1). Nevertheless, it is important to note that heat stress metrics, such as T_s, T_w, and sWBGT, do not represent the explicit physiological impacts of heat stress on individuals. Several epidemiological studies indicate that the relation between increased mortality and increased humidity in summer can be highly nonlinear [e.g., (40)]. The degree to which the correct physiological sensitivities are represented in our T_s metric is conditioned on the results by the meta-analysis in (1) and the correct fit of our metric to those data. It should also be noted that the T_s relation does not explicitly account for the lag structure between exposure to heat stress and mortality and that, besides T and q, other meteorological variables, such as radiation and wind, can be influential for human heat stress (10, 15). Nonetheless, these variables covary with T and q, for instance, high incoming solar radiation tends to coincide with low relative humidity conditions and high temperature; hence, T_s may still indirectly reflect these effects.

Environmental factors modifying local thermal stress such as (in/outdoor) effects of buildings or vegetation and the spatiotemporal societal response to heatwaves are certainly important factors for human heat stress (10, 15). Real-life impacts also remain subject to individual adaptation through infrastructure, clothing, activity, acclimatization, etc. (41). It is important to consider that the relationship between health and meteorological conditions is applied here universally, and that while T_s is based on the global heatwave mortality inventory from (1), this inventory overrepresents mid-latitude

Table 1. The impact of soil moisture anomaly on extreme heatwaves. Afternoon heat stress temperature (T_s), temperature (T), specific humidity (q), relative humidity (RH), and wet-bulb temperature (T_w) during deadly heatwaves recorded by morning-afternoon weather balloon launches for which the daily-average T_s exceeds the deadly: threshold of $T_s = 27°C$ (see Fig. 1A). For each variable x, the impact of soil moisture anomaly (dw) during the heatwave compared to the average summer soil moisture d_wx is provided.

Event	Date	Station	Place	Lat [°]	Lon [°]	w [-]	T_s [°C]	T [°C]	q [g/kg]	RH [%]	T_w [°C]	dw [-]	d_wT_s [°C]	d_wT [°C]	d_wq [g/kg]	d_wRH [%]	d_wT_w [°C]
Chicago heatwave	11/7/1995	74455	Davenport, USA	41.61	−90.58	0.40	27.7	30.3	18.3	65.5	25.2	0.113	−0.06	−1.13	1.27	8.6	0.41
	12/7/1995	74455	Davenport, USA	41.61	−90.58	0.39	30.2	33.5	20.8	61.6	27.4	0.103	−0.05	−1.04	1.12	6.9	0.31
	15/7/1995	72403	Washington, USA	38.97	−77.45	0.20	29.2	35.4	16.2	43.3	25.5	−0.026	−0.06	1.14	−1.13	−6.3	−0.32
	16/8/1995	72248	Shreveport, USA	32.45	−93.77	0.20	27.8	35.7	13.2	34.6	23.9	−0.017	−0.15	1.12	−1.04	−5.3	−0.33
	17/8/1995	72248	Shreveport, USA	32.45	−93.77	0.19	27.8	36.8	12.4	30.7	23.7	−0.020	−0.28	1.31	−1.29	−5.9	−0.46
	18/8/1995	72248	Shreveport, USA	32.45	−93.77	0.19	28.0	36.8	12.9	31.9	24.0	−0.021	−0.32	1.24	−1.36	−6.1	−0.51
Dallas humid heat	25/7/1997	72248	Shreveport, USA	32.45	−93.77	0.20	27.9	33.6	14.9	44.7	24.3	−0.013	−0.17	0.73	−1.01	−5.2	−0.39
	26/7/1997	72248	Shreveport, USA	32.45	−93.77	0.20	27.3	34.3	13.2	37.6	23.5	−0.016	−0.21	0.87	−1.03	−5.1	−0.39
Eastern U.S. heatwave	27/7/1999	72558	Omaha, USA	41.31	−96.36	0.40	28.5	31.5	19.3	63.2	25.8	0.112	0.14	−1.14	1.74	9.6	0.65
	27/7/1999	74455	Davenport, USA	41.61	−90.58	0.25	27.1	30.8	16.2	56.1	24.0	−0.043	0.04	0.73	−0.77	−5.3	−0.24
Indian heatwave 2002	23/6/2002	42182	Delhi, India	28.58	77.2	0.20	28.7	39.6	13.0	26.5	24.6	−0.076	−1.71	2.10	−4.63	−14.3	−2.14
Northern U.S. heatwave 2006	17/7/2006	72248	Shreveport, USA	32.46	−93.78	0.19	29.3	36.8	15.2	37.8	25.4	−0.020	−0.14	1.33	−1.30	−6.6	−0.39
Asian heatwave 2007	21/6/2007	42667	Bohpal, India	23.28	77.35	0.36	27.9	34.4	15.1	40.5	24.1	0.022	0.08	−0.34	0.42	1.9	0.15
Northern Hemisphere heatwave	4/8/2010	74560	Lincoln, USA	40.15	−89.33	0.25	28.8	35.7	15.3	39.5	25.0	−0.016	−0.12	0.44	−0.58	−2.6	−0.22
Northern U.S. heatwave 2012	29/6/2012	74560	Lincoln, USA	40.15	−89.33	0.24	28.6	38.9	13.0	27.9	24.5	−0.027	−0.36	1.24	−1.34	−5.2	−0.50

regions. We also do not explicitly include the potential of human adaptation to local climate; yet, the findings in (*1*) show that the relationship between lethality, humidity, and temperature can, to a large extent, be generalized globally. Moreover, it is important to note that our analysis focuses on direct diurnal effects of soil desiccation on afternoon T and q and does not explicitly explore the legacy of soil desiccation on multiday atmospheric conditions nor night-time heat stress. It is well known that soil desiccation during the development of heatwaves may exacerbate T over multiple days (*4*) and extend this effect to downwind regions (*8*). From that perspective, one may expect a similar prolonged effect for q, with air becoming progressively drier in response to soil desiccation, potentially leading to a further beneficial influence on heat stress as the heatwave evolves. Thus, the local and diurnal feedbacks of soil desiccation on heat stress explored in this study likely represent lower estimates than those that would occur if large-scale and multiday feedbacks were considered. Last, soil drought can induce additional changes to the atmospheric flow and geospatial height over multiple days (*39*)—leading to either an oppression or enhancement of convection, clouds, and, hence, radiation (*42*–*45*)—which are not considered here.

Since dry soils tend to increase air temperature because of sensible heating [e.g., (*18*)], there is a common perception that dry soils during hot events exacerbate lethal heat stress, which is also suggested by the correlation between dry soils and high heat stress (compare Fig. 2A and Fig. 2D). However, that perception is disproved by our analyses, which provide evidence for the beneficial role of soil dryness against lethal heat stress once air humidity influences are considered. While the benefit of soil dryness is shown to be modest on diurnal time scales, these findings question the potential of recently proposed heatwave mitigation strategies involving surface and/or air moistening to increase evaporative cooling. Our results suggest that irrigation, in particular, can be counterproductive, increasing human heat burden despite its associated decrease in T. The intensification of irrigation during the past century was recently found to reduce human exposure to hot extremes and was consequently deemed as beneficial for billions of people (*23*). However, that assessment did not consider the associated increase in q. Our analysis demonstrates that an increase in morning soil moisture levels to field capacity, mimicking irrigation, leads to an overall increase in heat stress in the afternoon, since the benefit due to reduced T is outweighed by the influence of increased q (fig. S8, A and B). The detrimental effect of irrigation becomes stronger for regions with high aridity (fig. S8B) since the amount of water needed to reach field capacity is larger, resulting in a greater increase in evaporation (fig. S8C). These results are in line with a contemporaneous analysis for today's irrigation practices in India (*28*), where it was shown that T decreases in response to irrigation, but T_w and other heat stress metrics increase instead. Analogously, afforestation can lead to sustained levels of soil moisture and evaporation during heatwaves and increase shading (*46*), urban vegetation or green roofs can reduce urban heat islands (*26*, *46*), and misting systems during mass events also tend to maintain evaporation at the expense of reducing sensible heat (*27*). However, the effectiveness of forestry, urban greening, or misting systems to combat heat stress should be evaluated by considering the influence they have on q, not just on T. The observation-driven atmospheric modeling framework adopted here, as well as the proposed T_s diagnostic of human heat stress, may be used to reevaluate these practices and design effective heatwave adaptation and mitigation strategies in the future.

MATERIALS AND METHODS

This section presents the materials and methods that allow us to establish causal relationships between soil moisture conditions and human heat stress globally. First, the lethal heat stress metric is defined to provide a new objective measure of deadly heat stress based on a meta-analysis of heatwaves with excessive mortality globally. Second, we present the CLASS4GL atmospheric modeling framework to simulate the diurnal properties of the ABL, including temperature and humidity. Then, we describe the modeling experiments performed in this study. Last, we quantify the separate and combined effects of morning soil moisture and atmospheric conditions on afternoon temperature, humidity, and deadly heat stress during hot spells, based on different perturbation experiments with CLASS4GL. There, we also scrutinize the contributions from land-atmosphere feedbacks, such as entrainment of air from the free atmosphere during the ABL growth.

Human heat-stress temperatures and episodes

Following the meta-analysis by (*1*), we propose the lethal heat stress temperature T_s (°C) as

$$T_s = T_w + 4.5\left(1 - \left[\frac{RH}{100}\right]^2\right) \tag{1}$$

with the wet-bulb temperature being T_w (°C) and the relative humidity RH (%). The use of T_w, i.e., the temperature that an air parcel has when it is cooled at constant pressure by evaporation into it until humidity reaches saturation, resembles the thermoregulation process of a human body (*12*); through perspiration (evaporative cooling), the body discharges metabolic heat and prevents potentially fatal hyperthermia even when the air temperature is higher than the body's core temperature of ∼ 37°C (*14*). To adjust T_w for better reflecting heat stress conditions under low levels of relative humidity according to (*1*), the second term [i.e., $4.5 (1 - [RH/100]^2)$] has been added (see Fig. 1A). This term collapses to zero when RH reaches 100%, under which dissipation of metabolic heat through sweating becomes ineffective. Using this definition of T_s allows us to assess human heat stress under different meteorological conditions, as the isopleths of constant T_s resemble combinations of daily mean air temperature and relative humidity that lead to equal T_s. Thresholds of $T_s = 19$°C and $T_s = 27$°C agree with the empirically derived lethal (blue line in Fig. 1A) and "deadly" (red line in Fig. 1A) thresholds of heat stress in (*1*). (*1*) shows that air temperature and air humidity most accurately distinguished between past lethal and nonlethal heat episodes, whereas other meteorological parameters, including radiation and wind, only lead to minimal increases of accuracy. Therefore, we only considered air temperature and humidity in the analysis.

We define lethal hot spells as days during which the average T_s is not lower than 19°C, and its 90th percentile summer value is exceeded. Summer is defined per location as the three consecutive months with the highest average T_s. Values of T_s in Figs. 1 and 2 are calculated using temperature and specific humidity from the latest reanalysis of the European Centre for Medium-Range Weather Forecasts [ERA5; see (*47*)], with a spatial resolution of 0.25° and averaged over summer episodes from 1981 to 2015. Analogously, human heat stress days are defined using daily averaged temperature and humidity from ERA5. The annual lethal hot spell frequency in Fig. 1B is calculated using 12,381 balloon sounding pairs (morning/afternoon) from 60 stations worldwide (see Fig. 1C). These are aggregated over

continental regions with the highest number of observations during summers between 1981 and 2015, including the Western United States (2842 soundings; 9 stations), Eastern United States (2514 soundings; 17 stations), Europe (1935 soundings; 10 stations), Russian Federation (1546 soundings; 12 stations), and Middle East (828 soundings; 6 stations). Anomalies in Figs. 2 to 4 are calculated as the difference between lethal hot spells and average summer days.

CLASS4GL land-atmosphere modeling framework
The observation-based model simulations used to decipher the role of soil moisture on human heat stress are carried out with the CLASS4GL (29), an observation-constrained and deterministic bulk model of the ABL that interprets balloon soundings, satellite, and reanalysis data mechanistically. CLASS4GL consists of three modules: a conceptual bulk model for the ABL (CLASS) (48, 49), a data mining module, and an interface to connect these two. In CLASS, the ABL is represented by a single model layer, for which thermodynamic equations are solved, assuming that potential temperature (θ), specific humidity (q), and winds (u, v) are homogeneously distributed. The model is typically initialized in the morning and simulates the evolution of the ABL during the day, providing a means to gain process-based understanding of the effects of land and atmospheric conditions on the diurnal evolution of the ABL. CLASS simulates a wide range of processes such as ABL growth, entrainment of sensible heat and moisture, subsidence, turbulent exchanges of momentum, sensible heat and moisture between land surface and atmosphere, evaporation from land and vegetation, and sensible heat and moisture transport dynamics of the soil.

The model was recently upgraded with a representation of advection (as additional atmospheric forcing) and a constraint of land surface evaporative fraction through satellite-based estimates, to iteratively infer soil moisture (29). In the CLASS4GL framework, CLASS is initialized and constrained by a wide range of observations: around 15 million balloon soundings from the Integrated Global Radiosonde Archive (IGRA) (50), but also field campaigns (29), satellite-based soil moisture and evaporation from the Global Land Evaporation Amsterdam Model (GLEAM) (51, 52), and reanalysis data from ERA5 (47) and ERA-Interim (53) for the remaining variables, such as cloud fraction, advection rates, land cover, and vegetation properties, and for gap-filling observations.

Filtering for suitable balloon soundings according to (29) leaves 10,517 morning-afternoon pairs from 60 stations (see Fig. 1C) reporting T and q that are used to initialize and evaluate the model and to perform perturbation experiments. From these, 306 morning-afternoon pairs were launched during hot spells. The global balloon soundings are used for determining ABL parameters including not only boundary layer height, T, θ, q, u, and v but also the T, θ, q, u, and v jumps at the top of the ABL and their lapse rates varying with height in the free troposphere. In addition, static data from satellite data are prescribed for wilting point, water field capacity, and saturated water content from the Global Gridded Surfaces of Selected Soil Characteristics from the International Geosphere-Biosphere Programme (IGBP-DIS), leaf-area index from the Global Inventory Monitoring and Modeling System (GIMMS), fractional vegetation cover and albedo from the Moderate Resolution Imaging Spectroradiometer (MODIS) Vegetation Continuous Fields (MOD44B), and vegetation canopy height from Geoscience Laser Altimeter System (GLAS). Thermal parameters and soil-water retention curve parameters are based on global soil survey data from the Digital Soil Map

of the World (DSMW). Further details including references of the datasets can be found in section 2.3 and table 1 of (29), and a full overview of the model parameters in the CLASS4GL reference simulations can be found in table 2 of (29).

To increase the reliability of the results obtained with CLASS4GL, we conducted validation experiments, in which diurnal simulations initialized with morning profiles are validated with afternoon profiles from balloon soundings. Similar to the findings by (29)—in which average biases on the order of $-0.036°C$ hour^{-1} and 0.06 g kg^{-1} hour^{-1} for θ and q were reported—we find that CLASS4GL is able to reproduce the diurnal dynamics of the ABL reported by weather balloons. Furthermore, T, q, and T_s anomalies during hot spells are well reproduced from the weather balloons and reanalysis data (compare stars and dots with rectangles in Fig. 3, A to C). Biases increase as aridity increases, which is likely a result of overestimated land surface evaporation and underestimated sensible heat fluxes during dry conditions [fig. S4 and (29)]. The overall biases are, however, smaller than the feedbacks that were simulated in this study (fig. S4). These results provide confidence that CLASS4GL is capable to simulate the diurnal dynamics of the ABL including the effect of soil moisture anomalies on T and q.

Modeling experiments with CLASS4GL
To isolate the diurnal feedback of the surface-ABL evolution to dry soils during hot spells [excluding effects of distinct hot spell atmospheric forcing (e.g., clear sky conditions) on the surface-ABL evolution], we take the simulations of hot spells and subtract them with the same simulations but perturbing the initial (morning) soil moisture with its median over all summer days. To isolate the diurnal feedbacks during hot spells associated with distinct hot spell atmospheric forcing on the surface-ABL evolution (excluding dry soil effects), we take the simulations of hot spells and subtract them with the simulations of all summer days for which the model is still initialized with the morning soil moisture during hot spells.

The full summer climatology (based on the three hottest months in 1981–2015) is subdivided into two categories: lethal hot spell days and regular summer days. For each of these categories, the median morning soil moisture is calculated and serves as the soil moisture reference. Similarly, the reference morning atmospheric conditions are calculated—in contrast to the soil moisture, these conditions are not averaged, but the single day observations are used. The same is done for all other summer days (i.e., the median summer day soil moisture is calculated, and the climatology is sorted for average summer day forcing). To estimate the contribution of dry soils during hot spells, two model simulations with CLASS4GL are compared: a reference hot spell simulation (using consistent hot spell median soil moisture and hot spell atmospheric conditions) and a reference summer day soil moisture simulation (using the median summer day soil moisture but hot spell atmospheric conditions). The afternoon difference between these two simulations then indicates the diurnal feedback of the surface-ABL evolution induced by dry soils during hot spells.

Analogously, to estimate the contribution of feedbacks associated with the atmospheric conditions, the forcing data are perturbed. Therefore, the reference hot spell simulation, as explained above, is compared with simulations over all (no hot spell) summer days, but substituting morning soil moisture with the median hot spell soil moisture. As the atmospheric forcing is kept the same, these simulations represent average summer days not experiencing hot spell

conditions ("average summer day atmospheric conditions"). The difference between these two simulations then isolates the diurnal feedbacks associated with the atmospheric forcing during hot spells but excludes the dry soil effect. To isolate the diurnal response of the ABL to dry soils during hot spells—excluding effects of distinct hot spell atmospheric forcing (e.g., clear sky conditions) on the surface and ABL—we take the simulations of hot spells and subtract them with the same simulations but perturbing the initial (morning) soil moisture with its median over all summer days. To isolate the diurnal feedbacks during hot spells associated with distinct hot spell atmospheric forcings (excluding dry soil effects), we take the simulations of hot spells and subtract them from the simulations of all summer days for which the model is still initialized with the morning soil moisture during hot spells.

Diurnal feedbacks contributing to afternoon anomalies during hot spells

The anomalies (Δ) of a generic atmospheric variable ψ (as shown for T, q, and T_s in Fig. 3) are calculated as the difference between lethal hot spells (s) and regular summer days (c)

$$\Delta\psi = \psi^s - \psi^c \qquad (2)$$

where

$$\psi^s = \frac{1}{n^s}\sum_{i=1}^{n^s}\psi_i \qquad (3)$$

and

$$\psi^c = \frac{1}{n^c}\sum_{i=1}^{n^c}\psi_i \qquad (4)$$

for all n^s hot spells and the remaining n^c summer days at each of the 60 balloon sounding stations.

Using CLASS4GL, the afternoon anomalies (Δ) can be subdivided into the anomalies that are already evident in the morning ($\Delta\psi_{morning}$) and the diurnal contributions (d) associated with soil moisture feedbacks ($d_w\psi$), atmospheric feedbacks ($d_a\psi$), and synergy feedbacks ($d_{w-a}\psi$)

$$\Delta\psi_{afternoon} = \Delta\psi_{morning} + d_w\psi + d_a\psi + d_{w-a}\psi \qquad (5)$$

To disentangle the feedback processes that contribute to the afternoon anomalies, we perform perturbation experiments for each station separately. To estimate the contribution of dry soils during hot spells, we replace the soil moisture during hot spells with the median summer day soil moisture w^c in CLASS4GL and rerun the diurnal simulations using the atmospheric forcing of all human heat stress days. The resulting feedback is then calculated as the difference

$$d_w\psi = \psi^s_{afternoon}(w) - \psi^s_{afternoon}(w^c) \qquad (6)$$

This illustrates the temperature (or humidity) that the air would have without dry soils, but considering anomalous atmospheric conditions. The diurnal feedback associated with atmospheric conditions is estimated by rerunning CLASS4GL during all days (afternoon) but initializing it with the morning soil moisture during hot spells (w^s)

$$d_a\psi = \left[\psi^s_{afternoon}(w) - \psi^c_{afternoon}(w^s)\right] - \left[\psi^s_{morning} - \psi^c_{morning}\right] \qquad (7)$$

illustrating the temperature or humidity that the air would have during nonstress episodes, but if soils were dry. The remaining contribution required to explain the diurnal anomalies arises from simultaneous feedbacks (considering the diurnal atmospheric contribution and the soil-moisture contribution simultaneously). This diurnal synergy feedback is calculated as

$$d_{w-a}\psi = \left[\psi^c_{afternoon}(w^s) - \psi^c_{afternoon}(w)\right] - \left[\psi^s_{afternoon}(w) - \psi^s_{afternoon}(w^c)\right] \qquad (8)$$

and illustrates the difference in diurnal response to anomalous soil moisture between simulations of typical summer days and simulations of hot spells (or alternatively, the difference in diurnal response to anomalous atmospheric conditions between the simulations with typical summer soil moisture and the simulations with hot spell soil moisture). For heat stress temperature (T_s), Eq. 6 yields

$$d_w T_s = T^s_{s,afternoon}(w) - T^s_{s,afternoon}(w^c) \qquad (9)$$

This total effect of soil moisture anomalies on heat stress temperatures can further be attributed to the individual feedbacks via temperature and humidity, i.e.

$$d_w T_s|_q = T^s_{s,afternoon}(w) - T^s_{s,afternoon}(T(w^c), q(w)) \qquad (10)$$

and

$$d_w T_s|_T = T^s_{s,afternoon}(w) - T^s_{s,afternoon}(T(w), q(w^c)) \qquad (11)$$

where the former is calculated by keeping afternoon-specific humidity unperturbed, and the latter by keeping the afternoon temperature unperturbed. Despite combining air temperature and specific humidity from different experiments, relative humidity did not exceed the saturation limit of 100%, which ensures consistency in the calculations. The red and blue lines and shadings in Fig. 4B show the impact of temperature feedbacks to soil desiccation on T_s (Eq. 10) and the impact of humidity feedbacks to soil desiccation on T_s, respectively. The orange line and shading in Fig. 4B show the net impact of compound soil droughts during hot spells on human heat stress (Eq. 9).

The diurnal soil moisture contribution $d_w\psi$ can further be subdivided into direct (surface) feedbacks arising from dry soils and indirect (upper air) feedbacks induced by dry soils via entrainment of warm and dry air from the free troposphere. In CLASS, the entrainment fluxes of sensible heat and moisture are calculated by multiplying the entrainment velocity by the jumps in respective potential temperature (θ) and q at the ABL top. The entrainment velocity is acquired by dividing the negative of the virtual potential temperature entrainment flux by the virtual potential temperature jump at the ABL top. The entrainment flux of virtual potential temperature is assumed to be a fixed fraction (0.2) of the surface flux of virtual potential temperature to which the shear-driven entrainment flux is added (*29*). To quantify the feedbacks associated with dry soils, we perform two additional perturbation experiments of hot spells, in which we perturb the moisture and sensible heat entrainment fluxes in CLASS4GL, respectively. Analogously to the previous experiments, we can then subdivide the soil moisture contribution further as

$$d_w\psi = d_{w,direct}\psi + d_{w,q:ent}\psi + d_{w,\theta:ent}\psi \qquad (12)$$

into the direct soil moisture feedback ($d_{w,\text{direct}}\psi$) and the subsequent feedbacks through entrainment of hot ($d_{w,\theta\text{:ent}}\psi$) and dry ($d_{w,q\text{:ent}}\psi$) air. To estimate $d_{w,q\text{:ent}}\psi$, the diurnal time series of moisture entrainment $V'_z q'_e$ is replaced with that of the perturbation experiment, considering soil moisture of average summer days, so that the corresponding feedback can be calculated as

$$
\begin{aligned}
d_{w,q\text{:ent}}\psi \ = \ &\psi^s_{\text{afternoon}}(w^s, V'_z q'_e(w^s), V'_z \theta'_e(w^s)) \\
&- \psi^s_{\text{afternoon}}(w^s, V'_z q'_e(w^c), V'_z \theta'_e(w^s))
\end{aligned}
\tag{13}
$$

and represents the feedback of dry air entrainment induced by anomalously dry soils. Analogously, the feedback associated with the entrainment of hot air is calculated as

$$
\begin{aligned}
d_{w,\theta\text{:ent}}\psi \ = \ &\psi^s_{\text{afternoon}}(w^s, V'_z q'_e(w^c), V'_z \theta'_e(w^s)) \\
&- \psi^s_{\text{afternoon}}(w^s, V'_z q'_e(w^c), V'_z \theta'_e(w^c))
\end{aligned}
\tag{14}
$$

by replacing the sensible heat entrainment $V'_z \theta'_e$ during hot spells with sensible heat entrainment during average summer days. The residual of both

$$
\begin{aligned}
d_{w,\text{direct}}\psi \ = \ &\psi^s_{\text{afternoon}}(w^s, V'_z q'_e(w^c), V'_z \theta'_e(w^c)) \\
&- \psi^s_{\text{afternoon}}(w^c, V'_z q'_e(w^c), V'_z \theta'_e(w^c))
\end{aligned}
\tag{15}
$$

reflects the direct impact of anomalously dry soils during human heat stress periods on ψ (i.e., T, q, or T_s).

While the experimental design accounts for feedbacks related to the dynamics of land conditions and the ABL (including changes in surface energy fluxes and upper air entrainment), other feedbacks related to atmospheric conditions that are considered as forcing (including clouds and advection) are not considered.

SUPPLEMENTARY MATERIALS

Supplementary material for this article is available at https://science.org/doi/10.1126/sciadv.abe6653

REFERENCES AND NOTES

1. C. Mora, B. Dousset, I. R. Caldwell, F. E. Powell, R. C. Geronimo, C. R. Bielecki, C. W. W. Counsell, B. S. Dietrich, E. T. Johnston, L. V. Louis, M. P. Lucas, M. M. McKenzie, A. G. Shea, H. Tseng, T. W. Giambelluca, L. R. Leon, E. Hawkins, C. Trauernicht, Global risk of deadly heat. *Nat. Clim. Chang.* **7**, 501–506 (2017).
2. *Atlas of Mortality and Economic Losses from Weather, Climate and Water Extremes (1979–2012)* (WMO No. 1123, World Meteorological Oranization, 2014).
3. F. Chiang, O. Mazdiyasni, A. AghaKouchak, Amplified warming of droughts in southern United States in observations and model simulations. *Sci. Adv.* **4**, eaat2380 (2018).
4. D. G. Miralles, A. J. Teuling, C. C. van Heerwaarden, J. Vilà-Guerau de Arellano, Mega-heatwave temperatures due to combined soil desiccation and atmospheric heat accumulation. *Nat. Geosci.* **7**, 345–349 (2014).
5. D. G. Miralles, P. Gentine, S. I. Seneviratne, A. J. Teuling, Land-atmospheric feedbacks during droughts and heatwaves: State of the science and current challenges. *Ann. N. Y. Acad. Sci.* **1463**, 19–35 (2018).
6. P. A. Dirmeyer, B. A. Cash, J. L. Kinter, T. Stan, T. Jung, L. Marx, P. Towers, N. Wedi, J. M. Adams, E. L. Altshuler, B. Huang, E. K. Jin, J. Manganello, Evidence for enhanced land–atmosphere feedback in a warming climate. *J. Hydrometeorol.* **13**, 981–995 (2012).
7. S. I. Seneviratne, T. Corti, E. L. Davin, M. Hirschi, E. B. Jaeger, I. Lehner, B. Orlowsky, A. J. Teuling, Investigating soil moisture–climate interactions in a changing climate: A review. *Earth Sci. Rev.* **99**, 125–161 (2010).
8. D. L. Schumacher, J. Keune, C. C. van Heerwaarden, J. Vilà-Guerau de Arellano, A. J. Teuling, D. G. Miralles, Amplification of mega-heatwaves through heat torrents fuelled by upwind drought. *Nat. Geosci.* **12**, 712–717 (2019).
9. M. M. Vogel, R. Orth, F. Cheruy, S. Hagemann, R. Lorenz, B. J. J. M. van den Hurk, S. I. Seneviratne, Regional amplification of projected changes in extreme temperatures strongly controlled by soil moisture-temperature feedbacks. *Geophys. Res. Lett.* **44**, 1511–1519 (2017).
10. J. R. Buzan, M. Huber, Moist Heat Stress on a Hotter Earth. *Annu. Rev. Earth Planet. Sci.* **48**, 623–655 (2020).
11. T. Matthews, Humid heat and climate change. *Progr. Phys. Geogr.* **42**, 391–405 (2018).
12. G. A. Meehl, C. Tebaldi, More intense, more frequent, and longer lasting heat waves in the 21st century. *Science* **305**, 994–997 (2004).
13. J. S. Pal, E. A. B. Eltahir, Future temperature in southwest Asia projected to exceed a threshold for human adaptability. *Nat. Clim. Chang.* **6**, 197–200 (2016).
14. S. C. Sherwood, M. Huber, An adaptability limit to climate change due to heat stress. *Proc. Natl. Acad. Sci. U.S.A.* **107**, 9552–9555 (2010).
15. J. R. Buzan, K. Oleson, M. Huber, Implementation and comparison of a suite of heat stress metrics within the Community Land Model version 4.5. *Geosci. Model Dev.* **8**, 151–170 (2015).
16. M. Hirschi, S. I. Seneviratne, V. Alexandrov, F. Boberg, C. Boroneant, O. B. Christensen, H. Formayer, B. Orlowsky, P. Stepanek, Observational evidence for soil-moisture impact on hot extremes in southeastern Europe. *Nat. Geosci.* **4**, 17–21 (2011).
17. L. Alexander, Extreme heat rooted in dry soils. *Nat. Geosci.* **4**, 12–13 (2011).
18. D. G. Miralles, M. J. van den Berg, A. J. Teuling, R. A. M. de Jeu, Soil moisture temperature coupling: A multiscale observational analysis. *Geophys. Res. Lett.* **39**, L21707 (2012).
19. S. Zhou, A. P. Williams, A. M. Berg, B. I. Cook, Y. Zhang, S. Hagemann, R. Lorenz, S. I. Seneviratne, P. Gentine, Land–atmosphere feedbacks exacerbate concurrent soil drought and atmospheric aridity. *Proc. Natl. Acad. Sci. U.S.A.* **116**, 18848–18853 (2019).
20. B. N. Sulman, D. T. Roman, K. Yi, L. Wang, R. P. Phillips, K. A. Novick, High atmospheric demand for water can limit forest carbon uptake and transpiration as severely as dry soil. *Geophys. Res. Lett.* **43**, 9686–9695 (2016).
21. C. C. van Heerwaarden, J. P. Mellado, A. de Lozar, Scaling laws for the heterogeneously heated free convective boundary layer. *J. Atmos. Sci.* **71**, 3975–4000 (2014).
22. C. C. van Heerwaarden, A. J. Teuling, Disentangling the response of forest and grassland energy exchange to heatwaves under idealized land–atmosphere coupling. *Biogeosciences* **11**, 6159–6171 (2014).
23. W. Thiery, A. J. Visser, E. M. Fischer, M. Hauser, A. L. Hirsch, D. M. Lawrence, Q. Lejeune, E. L. Davin, S. I. Seneviratne, Warming of hot extremes alleviated by expanding irrigation. *Nat. Commun.* **11**, 290 (2020).
24. M. J. Puma, B. I. Cook, Effects of irrigation on global climate during the 20th century. *J. Geophys. Res. Atmos.* **115**, D16120 (2010).
25. E. L. Davin, D. Rechid, M. Breil, R. M. Cardoso, E. Coppola, P. Hoffmann, L. L. Jach, E. Katragkou, N. de Noblet-Ducoudré, K. Radtke, M. Raffa, P. M. M. Soares, G. Sofiadis, S. Strada, G. Strandberg, M. H. Tölle, K. Warrach-Sagi, V. Wulfmeyer, Biogeophysical impacts of forestation in Europe: First results from the LUCAS (Land Use and Climate Across Scales) regional climate model intercomparison. *Earth Syst. Dynam.* **11**, 183–200 (2020).
26. E. S. Krayenhoff, M. Moustaoui, A. M. Broadbent, V. Gupta, M. Georgescu, Diurnal interaction between urban expansion, climate change and adaptation in US cities. *Nat. Clim. Chang.* **8**, 1097–1103 (2018).
27. S. Kang, J. S. Pal, E. A. B. Eltahir, Future heat stress during Muslim pilgrimage (Hajj) projected to exceed 'extreme danger' levels. *Res. Lett.* **46**, 10094–10100 (2019).
28. V. Mishra, A. K. Ambika, A. Asoka, S. Aadhar, J. Buzan, R. Kumar, M. Huber, Moist heat stress extremes in India enhanced by irrigation. *Nat. Geosci.* **13**, 722–728 (2020).
29. H. Wouters, I. Y. Petrova, C. C. van Heerwaarden, J. Vilà-Guerau de Arellano, A. J. Teuling, V. Meulenberg, J. A. Santanello, D. G. Miralles, Atmospheric boundary layer dynamics from balloon soundings worldwide: CLASS4GL v1.0. *Geosci. Model Dev.* **12**, 2139–2153 (2019).
30. Q. Kong, S. B. Guerreiro, S. Blenkinsop, X.-F. Li, H. J. Fowler, Increases in summertime concurrent drought and heatwave in Eastern China. *Weather Clim. Extrem.* **28**, 100242 (2020).
31. L. M. Rasmijn, G. van der Schrier, R. Bintanja, J. Barkmeijer, A. Sterl, W. Hazeleger, Future equivalent of 2010 Russian heatwave intensified by weakening soil moisture constraints. *Nat. Clim. Chang.* **8**, 381–385 (2018).
32. P. Greve, B. Orlowsky, B. Mueller, J. Sheffield, M. Reichstein, S. I. Seneviratne, Global assessment of trends in wetting and drying over land. *Nat. Geosci.* **7**, 716–721 (2014).
33. S. E. Perkins, L. V. Alexander, On the measurement of heat waves. *J. Climate* **26**, 4500–4517 (2013).
34. R. D. Koster, Y. C. Sud, Z. Guo, P. A. Dirmeyer, G. Bonan, K. W. Oleson, E. Chan, D. Verseghy, P. Cox, H. Davies, E. Kowalczyk, C. T. Gordon, S. Kanae, D. Lawrence, P. Liu, D. Mocko, C.-H. Lu, K. Mitchell, S. Malyshev, B. McAvaney, T. Oki, T. Yamada, A. Pitman, C. M. Taylor, R. Vasic, Y. Xue, GLACE: The global land–atmosphere coupling experiment. Part I: Overview. *J. Hydrometeorol.* **7**, 590–610 (2006).
35. J. M. C. Denissen, R. Orth, H. Wouters, D. G. Miralles, C. C. van Heerwaarden, J. Vilà-Guerau de Arellano, A. J. Teuling, Soil moisture signature in global weather balloon soundings. *NPJ Clim. Atmos. Sci.* **4**, 13 (2021).
36. C. C. van Heerwaarden, J. Vilà-Guerau de Arellano, A. F. Moene, A. A. M. Holtslag, Interactions between dry-air entrainment, surface evaporation and convective boundary layer development. *Q. J. Roy. Meteorol. Soc.* **135**, 1277–1291 (2009).

37. Y. Qian, M. Huang, B. Yang, L. K. Berg, A modeling study of irrigation effects on surface fluxes and land–air–cloud interactions in the Southern Great Plains. *J. Hydrometeorol.* **14**, 700–721 (2013).

38. M. Segal, Z. Pan, R. W. Turner, E. S. Takle, On the potential impact of irrigated areas in North America on summer rainfall caused by large-scale systems. *J. Appl. Meteor.* **37**, 325–331 (1998).

39. J. S. Pal, E. A. B. Eltahir, A feedback mechanism between soil-moisture distribution and storm tracks. *Q. J. Roy. Meteorol. Soc.* **129**, 2279–2297 (2003).

40. B. Armstrong, F. Sera, A. M. Vicedo-Cabrera, R. Abrutzky, D. O. Åström, M. L. Bell, B.-Y. Chen, M. de Sousa Zanotti Stagliorio Coelho, P. M. Correa, T. N. Dang, M. H. Diaz, D. Van Dung, B. Forsberg, P. Goodman, Y.-L. L. Guo, Y. Guo, M. Hashizume, Y. Honda, E. Indermitte, C. Íñiguez, H. Kan, H. Kim, J. Kyselý, E. Lavigne, P. Michelozzi, H. Orru, N. V. Ortega, M. Pascal, M. S. Ragettli, P. H. N. Saldiva, J. Schwartz, M. Scortichini, X. Seposo, A. Tobias, S. Tong, A. Urban, C. De la Cruz Valencia, A. Zanobetti, A. Zeka, A. Gasparrini, The role of humidity in associations of high temperature with mortality: A multicountry, multicity study. *Environ. Health Perspect.* **127**, 97007 (2019).

41. S. C. Sheridan, M. J. Allen, Temporal trends in human vulnerability to excessive heat. *Environ. Res. Lett.* **13**, 043001 (2018).

42. J. S. Pal, E. A. B. Eltahir, Pathways relating soil moisture conditions to future summer rainfall within a model of the land–atmosphere system. *J. Climate* **14**, 1227–1242 (2001).

43. B. P. Guillod, B. Orlowsky, D. G. Miralles, A. J. Teuling, S. I. Seneviratne, Reconciling spatial and temporal soil moisture effects on afternoon rainfall. *Nat. Commun.* **6**, 6443 (2015).

44. C. M. Taylor, R. A. M. de Jeu, F. Guichard, P. P. Harris, W. A. Dorigo, Afternoon rain more likely over drier soils. *Nature* **489**, 423–426 (2012).

45. M. B. Ek, A. A. M. Holtslag, Influence of soil moisture on boundary layer cloud development. *J. Hydrometeorol.* **5**, 86–99 (2004).

46. A. Sharma, P. Conry, H. J. S. Fernando, A. F. Hamlet, J. J. Hellmann, F. Chen, Green and cool roofs to mitigate urban heat island effects in the Chicago metropolitan area: Evaluation with a regional climate model. *Environ. Res. Lett.* **11**, 064004 (2016).

47. H. Hersbach, B. Bell, P. Berrisford, S. Hirahara, A. Horányi, J. Muñoz-Sabater, J. Nicolas, C. Peubey, R. Radu, D. Schepers, A. Simmons, C. Soci, S. Abdalla, X. Abellan, G. Balsamo, P. Bechtold, G. Biavati, J. Bidlot, M. Bonavita, G. D. C. P. Dahlgren, D. Dee, M. Diamantakis, R. Dragani, J. Flemming, R. Forbes, M. Fuentes, A. Geer, L. Haimberger, S. Healy, R. J. Hogan, E. Hólm, M. Janisková, S. Keeley, P. Laloyaux, P. Lopez, C. Lupu, G. Radnoti, P. de Rosnay, I. Rozum, F. Vamborg, S. Villaume, J.-N. Thépaut, The ERA5 global reanalysis. *Q. J. Roy. Meteorol. Soc.* **146**, 1999–2049 (2020).

48. J. Vilà-Guerau de Arellano, C. C. van Heerwaarden, B. J. H. van Stratum, K. van den Dries, *Atmospheric Boundary Layer, Integrating Air Chemistry and Land Interactions* (Cambridge Univ. Press, New York, 2015), Ch. 1.

49. C. C. van Heerwaarden, J. Vilà-Guerau de Arellano, A. Gounou, F. Guichard, F. Couvreux, Understanding the daily cycle of evapotranspiration: A method to quantify the influence of forcings and feedbacks. *J. Hydrometeorol.* **11**, 1405–1422 (2010).

50. I. Durre, R. S. Vose, D. B. Wuertz, Overview of the integrated global radiosonde archive. *J. Climate* **19**, 53–68 (2006).

51. D. G. Miralles, T. R. H. Holmes, R. A. M. De Jeu, J. H. Gash, A. G. C. A. Meesters, A. J. Dolman, Global land-surface evaporation estimated from satellite-based observations. *Hydrol. Earth Syst. Sci.* **15**, 453–469 (2011).

52. B. Martens, D. G. Miralles, H. Lievens, R. van der Schalie, R. A. M. de Jeu, D. Fernández-Prieto, H. E. Beck, W. A. Dorigo, N. E. C. Vedwoest, GLEAM v3: Satellite-based land evaporation and root-zone soil moisture. *Geosci. Model Dev.* **10**, 1903–1925 (2017).

53. D. P. Dee, S. M. Uppala, A. J. Simmons, P. Berrisford, P. Poli, S. Kobayashi, U. Andrae, M. A. Balmaseda, G. Balsamo, P. Bauer, P. Bechtold, A. C. M. Beljaars, L. van de Berg, J. Bidlot, N. Bormann, C. Delsol, R. Dragani, M. Fuentes, A. J. Geer, L. Haimberger, S. B. Healy, H. Hersbach, E. V. Hólm, L. Isaksen, P. Kållberg, M. Köhler, M. Matricardi, A. P. McNally, B. M. Monge-Sanz, J. J. Morcrette, B. K. Park, C. Peubey, P. de Rosnay, C. Tavolato, J. N. Thépaut, F. Vitart, The ERA-Interim reanalysis: Configuration and performance of the data assimilation system. *Q. J. Roy. Meteorol. Soc.* **137**, 553–597 (2011).

54. H. Wouters, CLASS4GL model experiments for assessing the impact of soil drought on lethal heat stress using weather balloon observations; https://datadryad.org/stash/share/G0UTiHbE6osF1Vr0vYxTUN7FWNI0f0B8Y1j8RXRT41g.

Soil drought can mitigate deadly heat stress thanks to a reduction of air humidity

Hendrik WoutersJessica KeuneIrina Y. PetrovaChiel C. van HeerwaardenAdriaan J. TeulingJeremy S. PalJordi Vilà-Guerau de ArellanoDiego G. Miralles

View the article online
https://www.science.org/doi/10.1126/sciadv.abe6653
Permissions
https://www.science.org/help/reprints-and-permissions

Use of this article is subject to the Terms of service